

# Dose and irradiation time analysis of negative pi-meson therapy using particle and heavy ion transport code system (PHITS)

A.P. Muhammad<sup>1\*</sup>, A.W. Harto<sup>1</sup>, Y. Sardjono<sup>2</sup>, G.S. Wijaya<sup>2</sup>, Z. Ismail<sup>2</sup>,  
I.M. Triatmoko<sup>2</sup>, Y. Kasesaz<sup>3</sup>

<sup>1</sup>Department of Nuclear Engineering and Engineering Physics, Faculty of Engineering, Universitas Gadjah Mada, 2  
Grafika Street, Yogyakarta 55281, Indonesia

<sup>2</sup>Research Center for Accelerator Technology, National Research and Innovation Agency Indonesia, Indonesia

<sup>3</sup>Nuclear Science and Technology Research Institute (NSTRI), Tehran, Iran

## ► Original article

### \*Corresponding author:

Andhika Pinastika Muhammad

### E-mail:

andhika.pinastika@mail.ugm.ac.id

Received: July 2022

Final revised: April 2023

Accepted: April 2023

Int. J. Radiat. Res., October 2023;  
21(4): 653-661

DOI: 10.52547/ijrr.21.4.8

**Keywords:** Dose, glioblastoma multiforme, irradiation time, negative pi-meson therapy.

## ABSTRACT

**Background:** Minimizing the radiation side effects in cancer therapy has become one of the major challenges in radiotherapy, especially if the cancer is located in vital organs such as the brain. Negative pi-meson-based therapy is one method of radiotherapy that allows cancer to receive a high radiation dose while the surrounding normal tissue receives a low radiation dose. This research aims to analyze negative pi-meson therapy's dose and irradiation time in glioblastoma multiforme. **Material and Methods:** Simulation-based research is conducted using the PHITS program. The source used is a negative pion beam with an intensity of  $2.5 \times 10^8$  pions/second with an energy of 30 MeV to 60 MeV with an interval of 1 MeV. The negative pion energy, which has the maximum dose rate in the cancer target area, was optimized to obtain the weighting factors and irradiation time. The irradiation was carried out in 30 fractions with the dose per fraction of 2 Gy. **Results:** Irradiation time per fraction obtained was 194.91 seconds. The organ at risks (OARs) analyzed in this research were soft tissue, skin, brain, and cervical spinal cord. The doses received by the OAR are 0.2641 Gy, 0.7645 Gy, 7.3295 Gy, and 0.075 Gy, respectively. **Conclusions:** In summary, negative pi-meson therapy has the potential to minimize radiation dose to healthy tissue while cancer still receives high-dose radiation. However, it is necessary to compare negative pi-meson therapy and other radiotherapy methods to determine the strengths and weaknesses of each method.

## INTRODUCTION

According to International Agency for Research on Cancer, in 2020, there were 19,292,790 new cancer cases worldwide, where 308,102 of them were cases of brain and nervous tissue cancer <sup>(1)</sup>. Regarding brain and nervous tissue cancer, glioblastoma multiforme (GBM) is the most malignant cancer and has a high growth rate. GBM cases are estimated to be 3.21 per 100,000 population and tend to affect more men compared to women, with an average age of 64 years <sup>(2)</sup>. Glioma is a primary brain tumour that arises from the brain-supporting cells, namely glial cells. The most common glioma is astrocytoma. Astrocytoma generally occurs in the cerebrum, specifically in the frontal lobe. Astrocytoma grade IV is called glioblastoma multiforme based on tumour histology. GBM is the most invasive glioma tumor because of its rapid growth and spread to other tissues <sup>(3)</sup>. GBM can be treated by surgery, chemotherapy, and radiotherapy. Radiotherapy treatment is carried out

by utilizing high-energy ionizing radiation to kill cancer cells <sup>(4)</sup>.

Radiotherapy aims to distribute a high dose of radiation to the cancer target and a low dose to the surrounding tissues. The ionizing radiation type used is one of the essential factors in achieving this aim. Radiotherapy that is widely used today uses photon radiation. However, the drawback of the photon radiotherapy method is that there is still a significant dose value at the surface and tail doses due to the attenuation characteristics of photon radiation <sup>(5)</sup>. Besides photon radiotherapy, another alternative for treating glioblastoma multiforme is to use Boron Neutron Capture Therapy (BNCT). However, one obstacle is ensuring that boron is evenly distributed only in cancer cells without spreading to healthy cells. In addition, the toxicity of the boron compounds used must also be considered. One method of radiotherapy that can localize the high doses to the target without using any compound is radiotherapy using a hadron particle. One of the hadron particles

used in radiotherapy was negative pi-meson. When entering the material, the negative pi-mesons distribute a small dose. Until a certain depth, the dose will significantly increase until it reaches the maximum dose. After that, a significant dose reduction will occur from the maximum to a value close to zero. When observed by the Percentage Depth Dose (PDD) curve, there will be a steep peak at a specific depth range. This curve peak is known as the Bragg peak<sup>(6)</sup>.

The negative pi-mesons have a Bragg peak where the dose is formed by protons, electrons,  $\alpha$  particles, and other nuclear fragments in the form of heavy nuclei from the interaction of the negative pion captured by the nucleus as it passes through the material. This phenomenon is called a star event. The negative pion energy utilized in radiotherapy can be adjusted to produce a combination of Bragg peaks that establish a dose profile with a horizontal peak towards cancer, so that cancer receives a balanced dose. Negative pion is produced from protons with 400 - 800 MeV energy from the accelerator pounded into the target materials such as graphite or beryllium. Then, separating the negative pion from the other particles requires a series of deflection and focus magnetic fields<sup>(7)</sup>. Compared to protons, negative pion has several advantages, namely the higher Relative Biological Effectiveness (RBE) value, lower Oxygen Enhancement Ratio (OER), and a better ratio of peak to plateau<sup>(8)</sup>. The clinical study by R. Greiner et al.<sup>(9)</sup> achieved a negative pion RBE value of 1.5 in the brain cancer cells. However, due to the high price and limited equipment availability for producing negative pion particles, protons are preferred to be developed and used in radiotherapy.

With the advancement of radiotherapy, from conventional to modern radiotherapy, that is, utilizing accelerator technology, negative pion may again be used as an alternative in radiotherapy treatment. Based on our studies, research on negative pi-mesons has been abandoned using a more specific period of time. Thus, this study was conducted to examine the characteristics of the use of negative pion in radiotherapy. This simulation-based research using Particle and Heavy Ion Transport Code System (PHITS) aims to determine negative pion therapy's dose distribution and irradiation time in glioblastoma multiforme cases.

## MATERIALS AND METHODS

Simulation-based research was conducted using PHITS software version 3.26, developed by Japan Atomic Energy Agency (JAEA).

### *The modelling of the negative pion extraction system*

The negative pion extraction system is customized to determine the negative pion output characteristics

produced from the interaction of high-energy protons toward the target material. The extraction system starts from the proton output from the accelerator that is pounded into the beryllium to the negative pion output channel. The proton used in this system is a proton with 500 MeV of energy with 1 mA of current. The protons pound a cylindrical beryllium target. The negative pion extraction channel is a cylindrical vacuum channel equipped with a boron carbide shielding as a neutron bar and lead as a photon bar. The particles produced from the interaction of high-energy protons and the target direct to an isotropic phenomenon. Therefore, shielding is provided as depleted uranium covering the beryllium target to deliver the particle result.

Furthermore, to separate the negative pion from the other particles produced, it uses a series of dipole magnetic fields so that the negative pion turns towards the channel output, while other particles having the opposite charge to the negative pion turn towards the opposite direction. After that, a quadrupole magnetic field should focus on the deflected negative pion beam. The tally in a tally *t-track* with a *reg* (region) type of *mesh* functions to get the flux value of each particle in the extraction system output. The expected characteristics of the output beam are a mono-energy, convergent, contamination-free negative pion beam with sufficient intensity to be used in radiotherapy.

### *The simulation of the negative pion range in water*

Simulation of the negative pion in the water phantom is performed to obtain negative pion range data that will be used to determine the energy range used in the therapy. Then, the pion in the water resulting from the PHITS simulation is made into a graphic and compared visually with the negative pion range data from the reference<sup>(10)</sup>. The geometry of the water phantom is a cube 30 cm long on each side. The cube is composed of H<sub>2</sub>O liquid with a density of 0.998207 gram/cm<sup>3</sup> in an air chamber of 80% nitrogen and 20% oxygen and a density of 0.0012 gram/cm<sup>3</sup>. The negative pion energy simulated ranges from 10 to 100 MeV with 5 MeV intervals. The variation is determined by modifying the data from the reference graph so that the results can be compared.

The simulation was conducted using a tally *t-track* with an *r-z* type mesh with a radius of 0.5 cm at a depth of 0 cm to 30 cm, which was divided into 3000 mesh to obtain the negative pion radiation intensity value throughout the depth of negative pion penetration in the water. The range of negative pion is determined based on the depth with a radiation intensity of 50% of the negative pion intensity on the surface of the water phantom<sup>(11)</sup>.

### *The modelling of ORNL phantom and tumor target*

The phantom geometry was customized based on the phantom from the Oak Ridge National Laboratory

(ORNL) <sup>(12)</sup>. An adult male phantom is used based on statistical data stating that GBM cases generally occur more in adult males than in females. The ORNL phantom geometry used is only from the head to the neck. The geometry of the tumor target is irregularly shaped about 8 cm from the head's frontal surface. Moreover, there is also the geometry of CTV and PTV, which are adapted to a more exact shape, namely a ball. The geometry of the CTV is spherical with a radius of 2.75 cm or GTV plus a margin of 1 cm. Then, the geometry of PTV is spherical with a radius of 3.25 cm or PTV plus a margin of 0.5 cm. The composition of the component material and phantom density refers to the publication of ICRP 110 <sup>(13)</sup>. The tumor material composition refers to the journal article by Richard et al. <sup>(14)</sup>. In addition, a volume calculation of each tissue and organ geometry is carried out using a tally t-volume in PHITS. The calculated volume value is later defined in the volume section for further simulations. If the volume of each tissue or organ is not defined, PHITS will automatically provide a volume value of 1 cm<sup>3</sup> to the tissue or organ.

**The simulation of negative pion on ORNL phantom**

Negative pion simulations on ORNL phantom and tumor targets were conducted to obtain dose rates throughout the depth of the ORNL phantom for the various energy of negative pion. If only using one energy, only a small part of the cancer will be exposed to a high dose, namely in the depth range with a Bragg peak. Therefore, it needs a combination of Bragg peaks with various energy. The combination of Bragg peaks will provide a curve with a flat peak, called the Spread-Out Bragg Peak (SOBP) curve so that cancer will be exposed to a balanced dose from front to back. The energy range used for the simulation was based on the depth of the cancer target in the ORNL phantom and the simulation results of the negative pion range in the water phantom. The simulation was carried out from anterior to posterior or from the front to the back of the head with an irradiation distance of 10 cm from the scalp.

The simulation used a tally t-track with an r-z-type mesh in the radius according to the beam radius at 0 - 20 cm depth divided into 200 mesh to gain the particle absorption dose rate throughout the ORNL phantom depth. PHITS simulation will produce a dose rate in Gy/source by default. However, by adding the source intensity value in the coding, the PHITS output dose value will be Gy/second. In this simulation, the particle dose rates calculated are negative pion, negative muon, electrons, photons, neutrons, alpha, heavy nuclei, and protons.

**The therapy optimization**

Negative pion simulation on the ORNL phantom and volume target will generate particle dose rate data throughout the phantom depth. The data is used

to determine the energy range used for therapy and optimization. The energy level is negative pion energy that produces a peak dose rate in the depth range of the cancer target so that it forms SOBP. The optimized dose rate is the effective dose rate, which is the dose rate of each particle multiplied by its RBE value and summed. The optimization is conducted to make the volume target's received dose homogeneous.

If the effective dose rate at depth is *j* and energy is *i*, then they are denoted as *y<sub>j</sub>*, while the irradiation time for each negative pion energy is denoted as *z<sub>j</sub>*, the total effective dose of multi-energy irradiation at depth *j* (equation 1).

$$z_j = \sum_{i=1}^m y_{j,i} t_i \tag{1}$$

Equation 1 is a linear equation system. Each component can be converted into a matrix to form equation 2. The irradiation time for each negative pion energy (*t<sub>i</sub>*) can be obtained by answering equation 2 using the matrix multiplication as equation 3. This equation is for the entire depth of the cancer target. Thus, the value of *z<sub>j</sub>* is made uniform, that is, 2 Gy, the same as the dose per fraction that has been prescribed. *Y* is the matrix form of the effective dose rate, *T* is the matrix form of irradiation time, and *Z* is the matrix form of the total effective dose of multi-energy irradiation.

$$[Y][T] = [Z] \tag{2}$$

$$[T] = [Z]^{-1}[Z] \tag{3}$$

The total dose obtained is to form a flat-high SOBP curve at the cancer target. Then, it forms a lower curve at a depth of surrounding normal tissue. The results of the optimization of the dose received by cancer and surrounding normal tissue can be obtained through multi-energy simulations by assessing a weighting factor to each negative pion energy level, that is, as the negative pion flux fraction in the simulation. The weighting factor (*A<sub>i</sub>*) can be obtained by converting the irradiation time of each energy into a fraction (equation 4).

$$A_i = \frac{t_i}{\sum_{i=1}^m t_i} \tag{4}$$

Multi-energy simulations were conducted using a tally t-track with an r-z mesh to gain the absorbed dose rate of particles throughout the phantom depth, the xyz mesh to obtain the visualization of the dose distribution in the phantom, and the reg (region) mesh to obtain the dose rate in the target and the surrounding normal tissue. Similar to the previous simulation, the particle dose rates calculated in this multi-energy simulation are negative pion, negative muon, electrons, photons, neutrons, alpha, heavy nuclei, and protons.

### Result analysis

The value of the dose rate obtained from the simulation is the value of the absorbed dose rate ( $\dot{D}$ ). The absorbed dose rate must be converted to the effective dose rate ( $\dot{D}_{RBE}$ ) by multiplying the absorbed dose rate for each particle by its RBE value (equation 5). RBE for negative pion is divided into two, namely, the RBE plateau and the RBE peak. The  $RBE_{plateau}$  is the RBE value when the negative pion enters the medium with a small LET, while  $\dot{D}_{plateau}$  is the dose rate when the negative pion enters the medium.  $RBE_{peak}$  is the RBE value when the core captures a negative pion and a star event occurs, while  $\dot{D}_{peak}$  is the dose rate when a star event occurs.

$$\dot{D}_{RBE} = \dot{D}_{plateau} \times RBE_{plateau} + \dot{D}_{peak} \times RBE_{peak} \quad (5)$$

This study used the RBE plateau for negative pion particles and their decay products (negative muon and electrons) and photons. Thus,  $\dot{D}_{plateau}$  is the accumulation of negative pion, negative muon, and electron's dose rate. Then, the RBE peak is utilized for particles from the interaction of capturing pion, namely protons, neutrons, alpha, and heavy nuclei. Therefore,  $\dot{D}_{peak}$  is the accumulation of proton, neutron, alpha, and heavy nuclei's dose rate. Referring to the experiment of negative pion therapy conducted for astrocytoma cases <sup>(9)</sup>, the RBE plateau value in this study was 1, while the RBE peak value was 1.5.

$$\dot{D}_{RBE} = (\dot{D}_{pion} + \dot{D}_{muon} + \dot{D}_{elektron} + \dot{D}_{foton}) \times 1 + (\dot{D}_{proton} + \dot{D}_{neutron} + \dot{D}_{alfa} + \dot{D}_{nukleus}) \times 1.5 \quad (6)$$

The irradiation time per fraction has been obtained at the optimization stage by summing the irradiation time ( $t_i$ ) of each negative pion energy to achieve a dose of 2 Gy.

$$t = \sum_{i=1}^m t_i \quad (7)$$

The received dose of the target and surrounding normal tissue (D) can be obtained by multiplying the effective dose rate of each tissue by the therapeutic duration per fraction (t) and the number of fractions (n).

$$D = \dot{D}_{RBE} \times t \times n \quad (8)$$

For Clinical Tumor Volume (CTV) and Planning Target Volume (PTV), the received dose value has to be calculated differently due to the limitations of the PHITS. CTV should comprise Gross Tumor Volume (GTV) volume plus margin, and PTV should comprise CTV volume plus margin. However, the CTV and PTV volumes in the PHITS simulation are similar to their respective margins. Thus, the dose received by CTV ( $D_{CTV}$ ) can be calculated using the GTV volume ( $V_{GTV}$ ), dose received by GTV ( $D_{GTV}$ ), CTV volume based on simulation ( $V_{ctv}$ ), and dose received by CTV based on

simulation ( $D_{ctv}$ ).

$$D_{CTV} = \frac{V_{GTV} \times D_{GTV} + V_{ctv} \times D_{ctv}}{V_{GTV} + V_{ctv}} \quad (9)$$

Furthermore, the dose received by PTV ( $D_{PTV}$ ) can be calculated using the PTV volume based on simulation ( $V_{ptv}$ ) and the dose received by PTV based on simulation ( $D_{ptv}$ ).

$$D_{PTV} = \frac{V_{GTV} \times D_{GTV} + V_{ctv} \times D_{ctv} + V_{ptv} \times D_{ptv}}{V_{GTV} + V_{ctv} + V_{ptv}} \quad (10)$$

The dose calculation result is evaluated regarding whether the dose received by the target already meets the prescription and whether the dose received by surrounding normal tissue or Organ at Risk (OAR) exceeds each dose constraint. In validating the simulation results, PHITS performs calculations with a certain number of iterations to see the results of the interaction of particles in matter. The error value must be considered to ensure the calculation results are accurate and precise. The simulated data used is data that meets an error value below 0.05; this value indicates that from the many iterations of the calculation that has been carried out, the dose rate value obtained is the value that best represents the phenomenon that occurs in the medium simulated.

## RESULTS

### The result of the modelling of negative pion extraction system

Based on the PHITS simulation, the interaction between high-energy protons and a beryllium target produces various particles: neutrons, photons, alpha particles, and positive and negative pion. A series of magnetic fields divide the negative pion from other particles and determines the negative pion energy used in radiotherapy. The charge of negative pion is different from other particles. The negative pion will be deflected in the opposite direction from the other particles using a series of dipole magnetic fields, except for neutrons and photons with zero charges. In the model, the magnetic fields are in cells 71, 72, 73, 74 & 91 (figure 1).

The strength of the magnetic field will affect the negative pion deflection according to its energy level. Therefore, to ensure the negative pion to the expected energy, the strength of the magnetic field should be adjusted to the momentum of the negative pion particles and the energy. The separated negative pion in this system is negative pion with an energy of 80 MeV, the energy level generally utilized in negative pion therapy. The magnitude value of the magnetic field in this system is obtained through a trial-and-error simulation method until a suitable magnetic field strength is found to deflect and focus the 80 MeV negative pion.

Based on the simulation result, it gains the value of the particle flux at the extraction system output, the

flux in cell 84 (table 1). It is revealed that neutron and photon contaminants are at the beam's output with relatively high flux because the distance between the target and the output is very close. Based on the reference, the distance between the target and the output should be 8-10 meters, while only about 3 meters in the model. During the research, there were impediments in simulating the extraction system with large geometries. The simulation process runs over the capacity of the resource, so it takes much time. Hence, the negative pion beam output parameter for further simulations refers to the TRI University Meson Facility (TRIUMF) Biomedical Pion Channel (10,15), which has an output intensity of  $2.5 \times 10^8$  pion/s.

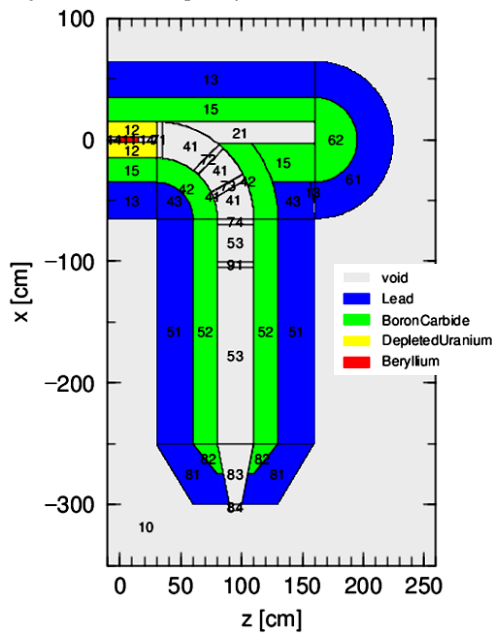


Figure 1. Negative pion extraction system.

Table 1. Particle flux on output system.

Particle	Flux (1/cm <sup>2</sup> /second)
Protons	0
Neutrons	$4.6146 \times 10^{11}$
Photons	$4.1287 \times 10^{11}$
Alpha	0
Pion+	0
Pion-	$6.1735 \times 10^9$

**The result of the simulation of the negative pion range in water**

Based on the PHITS simulation result, no negative pion intensity is precisely 50% of the water phantom surface intensity. So, the negative pion range is determined between two meshes that the intensity is greater than 50% and lesser than 50% of the surface intensity.

The negative pion has a smaller mass than the proton. Therefore the negative pion range is far

longer than the protons range in water with similar energy. In radiotherapy, the required negative pion energy commonly does not exceed 100 MeV.

The negative pion range data from the simulation is made into a graphic (figure 2) to be compared with the negative pion range data in the water set out in the reference (figure 3). Since the reference only has negative pion range data in a graphic, the simulation's absolute and relative error values cannot be calculated. The results can only be compared visually in graphical form. If the two graphs are compared, the negative pion range from the PHITS simulation is nearly similar to the negative pion range from the reference.

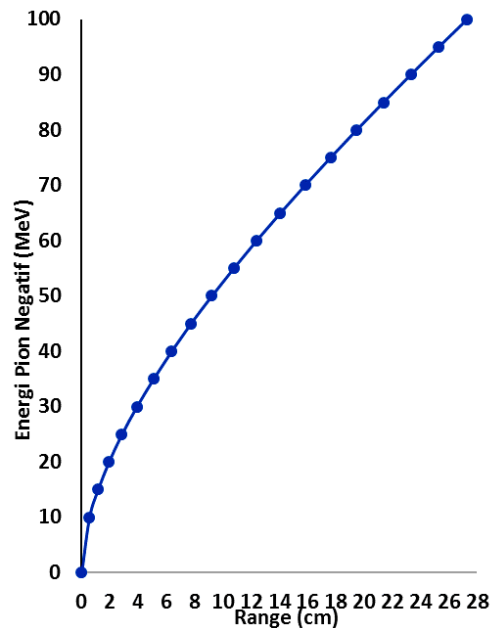


Figure 2. The graphic of negative pion range with different energy levels in water phantom (simulation result).

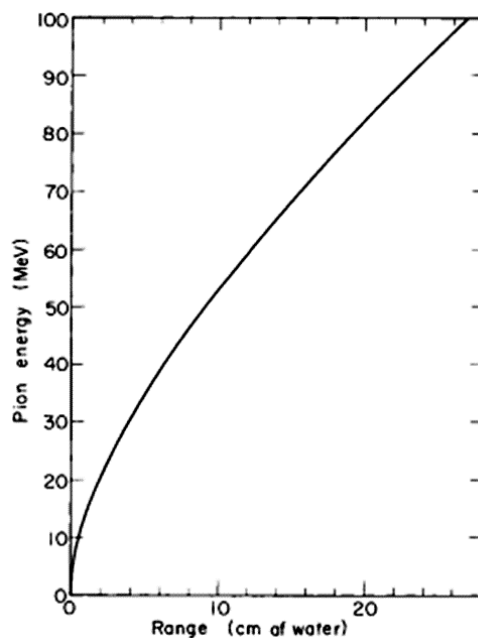


Figure 3. The graphic of negative pion range with different energy levels in water (reference) (10).

**The result of the modelling of ORNL phantom and tumor target**

The ORNL phantom and tumor targets in the simulation were successfully customized. It is proven by the zero errors when PHITS runs the geometry coding that has been generated, and there are no overlapping regions when the geometry is visualized in either two or three dimensions. The customized tissues and organs are the skin, the soft tissue of the head and neck, the cervical spine, the skull, and the brain. In the dose analysis stage, those tissues and organs would be analyzed as OAR, except the skull. The two-dimension visualization displays the phantom in axial, sagittal, and coronal planes. Each organ geometry has a different colour and each name description (figure 4 & 5).

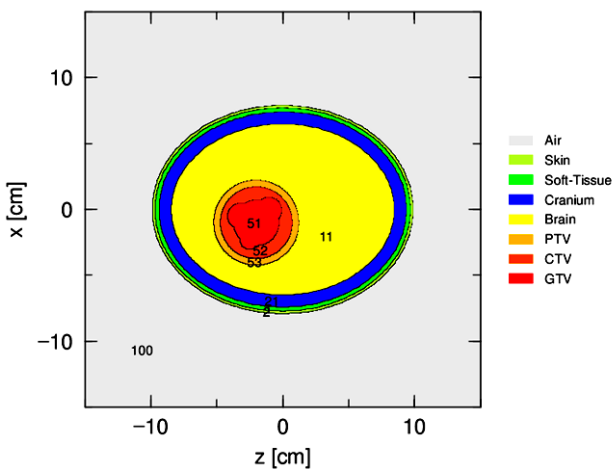


Figure 4. Axial plane of ORNL and tumor target.

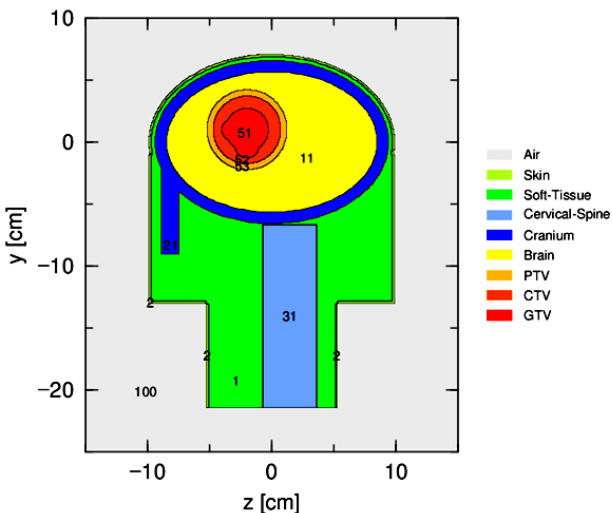


Figure 4. Axial plane of ORNL and tumor target.

**The result of the simulation of negative pion on ORNL phantom**

The negative pion simulation data on the ORNL phantom deliver the absorbed dose rate of each particle throughout the phantom depth. The absorbed dose rate is converted to the effective dose rate using Equation 4. The effective dose rate data gained is processed into a graphic (figure 6).

Based on the graphic, the maximum dose rate or Bragg peak will be deeper as the increasing negative pion energy. Moreover, the dose rate increase towards the maximum dose rate nearly occurs perpendicular. This is favourable in radiotherapy because the tissue in front of the target only receives a small dose. However, after reaching the maximum dose rate, the dose rate does not decrease drastically or perpendicular, but it decreases gradually as increasing depth until reaching zero. This phenomenon is caused by the geometrical surface of the head phantom exposed in this simulation being an ellipse and not flat hence, there is still normal tissue behind the target exposed to a pretty high dose.

The dose rate data can be used to determine the energy range used for therapy and optimization. The energy level is negative pion energy that generates a maximum dose rate in the cancer target depth range so that SOBP is formed. The target is at 4.75 – 11.25 cm of depth. Based on the result, the energy range in optimization and simulation of final therapy is 35 – 57 MeV.

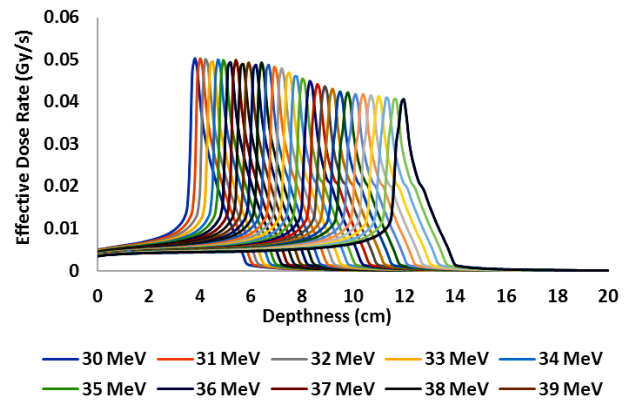


Figure 6. The graphic of the negative pion dose rates with different energy levels throughout the ORNL phantom depth.

**The result of the therapy optimization**

Therapy optimization is carried out, aiming that the cancer target gets a homogeneous dose throughout its depth. Optimization will produce a more homogeneous result delivered in all target depth points. Based on equation 3, only the square matrix can be inverted. Likewise, the optimization is only carried out at the target's depth point with a maximum dose rate. The weighting value of each energy is verified utilizing the SOBP curve.

Based on the optimization result, the total duration of irradiation per fraction is 192.41 seconds. According to the graphic, no hotspots were found throughout the target depth. Hotspot is a spot that receives a dose of more than 170% of the prescribed dose. In this case, the hotspot was 2.14 Gy. However, there is a coldspot on the target, namely the spot that receives a dose less than 95% of the prescribed dose. In this case, the coldspot was 1.9 Gy. The coldspot was at a depth of 10, 10.6, and 11.2 cm. Hence,

re-optimization is required by changing the irradiation duration for specific energy to resolve the coldspot issue. Re-optimization is carried out in the trial-and-error method.

Re-optimization was applied to the negative pion of 53 and 56 MeV energy by extending the irradiation duration for both energies. Re-optimization is carried out when avoiding the hotspots throughout the target depth. The re-optimization result successfully resolved the coldspot at a depth of 10 and 10.6 cm (figure 7). Then, there is still a coldspot at a depth of 11.2 cm. However, it is tolerable because the depth is near the edge between PTV and normal tissue, so it maintains the dose to keep low in the brain tissue behind the PTV. From the result, the irradiation duration per fraction obtained is 194.91 seconds.

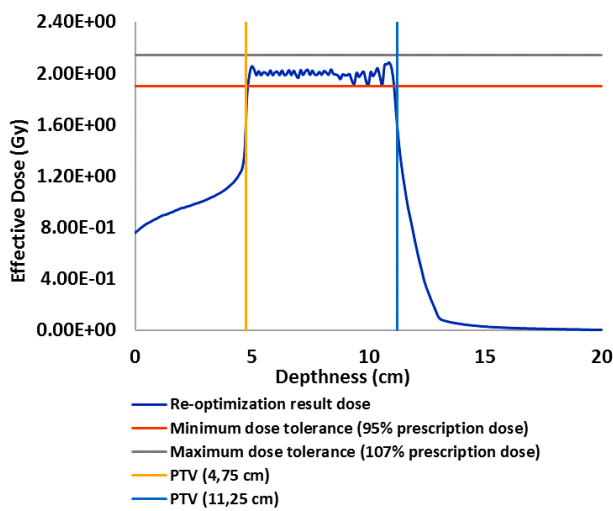


Figure 7. The graphic of effective dose rate resulting from re-optimization.

**Target and OAR received dose**

The received dose for the target and OAR was calculated from a multi-energy simulation utilizing the weighting factor of each negative pion energy from the optimization stage using equation 4. There are 23 discrete energy levels that were defined by the appropriate weighting factor. The data obtained from the multi-energy simulation are the absorption dose rates of negative pion particles, negative muons, electrons, photons, neutrons, alpha particles, heavy nuclei, and protons from each organ. The absorbed dose rate is converted to the effective dose rate using Equation 6. Then, the effective dose rate is multiplied by the irradiation duration and the number of fractions to gain each target's and OAR's received dose (table 2 & 3). In this study, the dose prescribed is 60 Gy, given in 30 fractions.

Table 2. The target's received dose. GTV: Gross Tumor Volume; CTV: Clinical Tumor Volume; PTV: Planning Target Volume.

Target	Dose per fraction (Gy)	Total dose (Gy)	Percentage of Prescribed Dose
GTV	2.0914	62.7406	104.57
CTV	2.0610	61.8294	103.05
PTV	2.0545	61.6364	102.73

Table 3. The received dose and dose constraint of the tissues and organs.

Tissue/Organ	Total Dose (Gy)	Dose Constraint
Soft tissue (head and neck)	0.2641	$D_{max} \leq 64.2$ Gy
Skin	0.7645	$D_{max} \leq 39.5$ Gy; $V36.5$ Gy < 10 cc
Brain	7.3295	$D_{max} < 60$ Gy
Cervical spine	0.075	$D_{max} \leq 50$ Gy
Skull	1.6168	-

The visualization of the distribution of the total absorbed dose rate was also simulated using PHITS and displayed in axial, sagittal, and coronal planes (figure 8, 9 & 10).

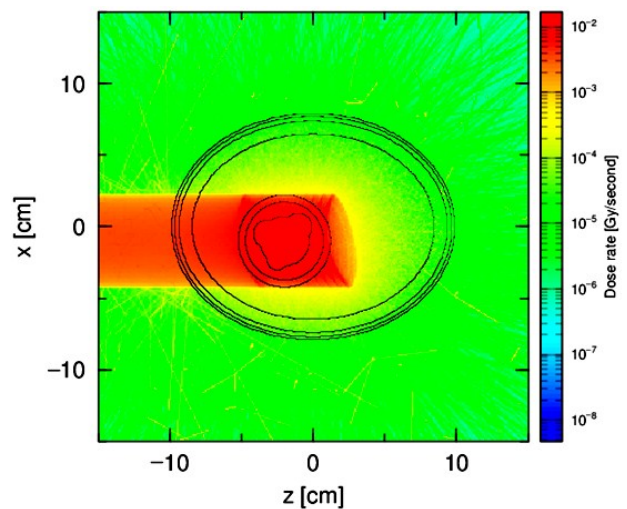


Figure 8. The distribution of the total absorbed dose rate in the axial plane.

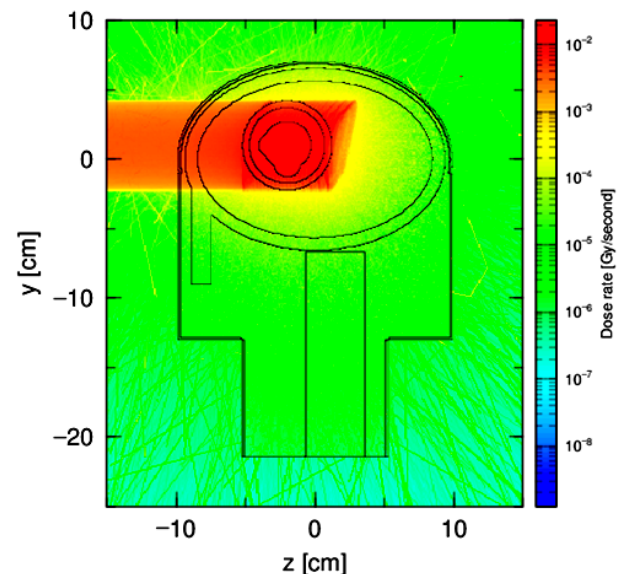
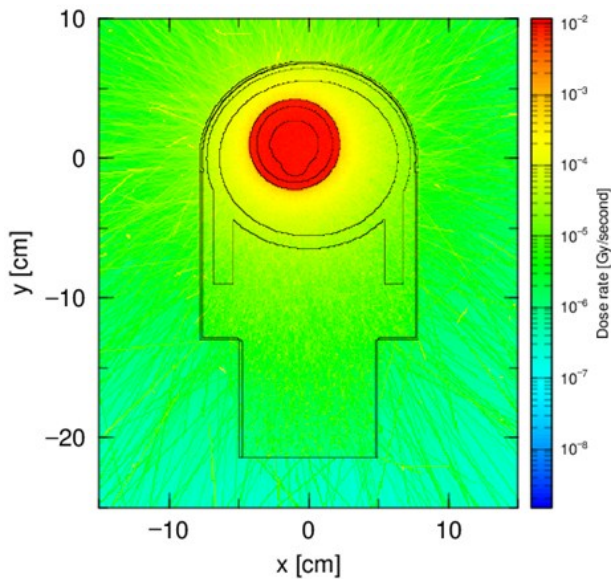


Figure 9. The distribution of the total absorbed dose rate in the sagittal plane.



**Figure 10.** The distribution of the total absorbed dose rate in the coronal plane.

## DISCUSSION

Based on the simulation result, the dose per fraction and the total dose received by GTV, CTV, and PTV are proportionate to the prescribed dose. These did not exceed the dose tolerance limit of more than 107% and less than 95% of the prescribed dose. When compared, GTV received the highest dose, CTV was in second place, and PTV was the lowest. It occurs as the dose received at various depth points, in the PTV margin area ranging from 4.75-5.25 cm and 10.75-11.25 cm, is near 95% of the prescribed dose, as shown in Figure 7. Thus, the average received dose of PTV is lower than GTV or CTV.

Aside from the received dose of the target, another indicator of radiotherapy success is the received dose of OAR. In this study, the organs and tissues reviewed as OAR were soft tissue (head and neck), skin, the brain, and the cervical spine. Each OAR has its own dose constraint. There are several references regarding dose constraints in radiotherapy. In this study, the dose constraint refers to the Quantitative Analysis of Normal Tissue Effects in the Clinic (QUANTEC) for conventional fractionation (1.8-2 Gy/fraction) <sup>(16)</sup>.

The soft tissue (body) dose constraint is that the maximum dose should not exceed 64.2 Gy or 107% of the target dose delivered. The average dose received by the head and neck soft tissue based on the PHITS simulation is 0.2641 Gy. Based on the data, the dose received by the soft tissues in the head and neck is far below the tolerance limit.

The skin dose constraint has two conditions: the maximum dose should not exceed 39.5 Gy, and the volume to receive the 36.5 Gy dose should not exceed 10 cc. The average dose received by the skin based on the PHITS simulation is 0.7645 Gy. Based on the data,

the dose received by the skin has already met the first condition. In the second condition, the Dose Volume Histogram (DVH) analysis is required to check whether the received dose has met the determined dose constraint. However, PHITS has yet to have that. Thus, the analysis of dose constraints for skin only utilizes the first condition. In the field, medical physicists generally only utilize one condition if there are several conditions of dose constraint for an organ. It is applied if it is difficult to meet all the conditions during the treatment planning.

The brain dose constraint is that the maximum dose should not exceed 60 Gy. Based on the PHITS simulation, the average dose received by the brain is 7.3295 Gy. Based on the data, the dose received by the brain is lower than the tolerance limit. Although the brain can receive a maximum dose that exceeds the dose constraint at a certain point, dose analysis can only be carried out using the available data due to the use of the non-voxel phantom and the limitations of PHITS.

The cervical spine dose constraint is that the maximum dose should not exceed 50 Gy. The average received dose for the cervical spine based on the PHITS simulation is 0.075 Gy. Based on the data, the dose received by the cervical spine is far below the tolerance limit. In general, the doses received by OAR in this simulation have already met each dose constraint.

In the axial and sagittal planes of visualization, it is revealed that the back part received a quite high dose rate at a depth of several centimeters. As explained before, it occurs because the geometric surface of the head phantom exposed in this simulation is an ellipse, not flat. Therefore, the brain volume behind the target receives a high dose. However, it is tolerable as the average dose in the brain is below the tolerance limit.

In another study, glioblastoma therapy based on carbon ion and BNCT using the SHIELD-HIT12A program <sup>(17)</sup> required 18.02 minutes to reach a dose of 52.6 Gy. BNCT took 133.8 minutes for a boron concentration of 35  $\mu\text{g}$  boron/g tissue. In proton-based cancer research using PHITS, it takes 73.65 seconds to reach a dose of 50 Gy <sup>(18)</sup>, while in the negative pi-meson study, it takes 194.91 seconds to reach a dose of 60 Gy. However, carbon ion therapy requires firing in a different direction because the dose given to healthy tissue before cancer exceeds the dose limit. In contrast, the BNCT, proton, and negative pi-meson methods it does not require fractionation because it has given a low-value dose to healthy tissue.

## CONCLUSION

In summary, negative pi-meson therapy has the potential to minimize radiation dose to healthy tissue while cancer still receives high-dose radiation. However, it is necessary to compare negative

pi-meson therapy and other radiotherapy methods to determine the strengths and weaknesses of each method.

#### ACKNOWLEDGEMENT

The official PHITS 3.26 license was utilized under the Japan Atomic Energy Agency (JAEA). The support from the Japan Atomic Energy Agency (JAEA) is appreciated with thanks.

**Conflicts of interests:** None.

**Ethical statement:** "Dose and irradiation time analysis of negative pi-meson therapy in glioblastoma multiforme using the PHITS program". All persons who meet authorship criteria are listed as authors. All authors certify that they have participated sufficiently in the work to take public responsibility for the content, including participation in the manuscript's concept, design, analysis, writing, or revision.

**Funding:** This research received no specific funding from public, commercial, or non-profit sector funding agencies.

**Author contribution:** Andhika P. Muhammad: making and executing the simulation, data analysis, and writing; Andang W. Harto & Yohannes Sardjono: study design, reviewing, and supervising; Zuhdi Ismail: revising and supervising; Gede S. Wijaya, Isman M. Triatmoko, & Yaser Kasesaz: supervising.

#### REFERENCES

1. GLOBOCAN (2020) Estimated number of new cases in 2020. International Agency for Research on Cancer. <https://gco.iarc.fr> (accessed January 20, 2022).
2. Anonymous (2021) Glioblastoma Multiforme. American Association of Neurological Surgeons. <https://www.aans.org/en/Patients/Neurosurgical-Conditions-and-Treatments/Glioblastoma-Multiforme> (accessed January 20, 2022).
3. Salles D, Laviola G, Malinverni AC de M, Stávale JN (2020) Pilocytic Astrocytoma: A Review of General, Clinical, and Molecular Characteristics. *J Child Neurol*, **35**: 852–8.
4. Michaelson NM and Connerney MA (2020) Glioblastoma multiforme that unusually present with radiographic dural tails: Questioning the diagnostic paradigm with a rare case report. *Radiol Case Rep*, **15**:1087–90.
5. Varatharaj C, Shwetha B, Rekha Reddy B, et al. (2016) Physical characteristics of photon and electron beams from a radiotherapy accelerator. *International Journal of Medical Research and Review*, **4**:1178–88.
6. D'ávilaununes M (2014) Hadron therapy physics and simulations. *New York: Springer*.
7. Yashar CM (2018) Basic principles in gynecologic radiotherapy. *Clinical Gynecologic Oncology, Elsevier Inc*, p. 586-605.e3.
8. Kugerman MM and Sternhagen CJ (1976) Radiation Oncology. *The Physiopathology of Cancer: Diagnosis, Treatment, Prevention*, **2**:135–81.
9. Greiner R, Blattmann H, Coray A, et al. (1990) Anaplastic astrocytoma and glioblastoma" pion irradiation with the dynamic conformation technique at the Swiss Institute for Nuclear Research (SIN). *Radiotherapy and Oncology*, **17**: 37–46.
10. Raju MR (1980) Heavy particle radiotherapy. *New York: Academic Press*.
11. Tsoulfanidis N and Landsberger S (2015) Measurement and detection of radiation. 4th ed. *New York: CRC Press*.
12. Krstic D and Nikezic D (2007) Input files with ORNL-mathematical phantoms of the human body for MCNP-4B. *Comput Phys Commun*, **176**: 33–7.
13. ICRP (2009) ICRP publication 110: Adult Reference Computational Phantoms. vol. 39. *Polestar Wheatons Ltd*.
14. Maughan RL, Chuba PJ, Porter AT, et al. (1997) The elemental composition of tumors: Kerma data for neutrons. *Med Phys*, **24**:1241–4.
15. Harrison RW and Lobb DE (1973) A negative pion beam transport channel for radiobiology and radiation therapy at triumph.
16. Marks LB, Yorke ED, Jackson A, et al. (2010) Use of normal tissue complication probability models in the clinic. *Int J Radiat Oncol Biol Phys*, **76**: S10–9.
17. William (2019) Dose and irradiation analysis on carbon ion radiotherapy toward boron neutron capture therapy using SHIELD-HIT12A program. *Universitas Gadjah Mada: Yogyakarta*.
18. Muhammad I (2022) Dose and irradiation time analysis of proton therapy in cervical cancer using PHITS. *Universitas Gadjah Mada: Yogyakarta*.

